APL Materials

Wave transport in 1D stealthy hyperuniform phononic materials made of non-resonant and resonant scatterers

Cite as: APL Mater. **9**, 101101 (2021); https://doi.org/10.1063/5.0059928
Submitted: 14 June 2021 • Accepted: 09 September 2021 • Published Online: 04 October 2021

V. Romero-García, É. Chéron, S. Kuznetsova, et al.

Wave transport in 1D stealthy hyperuniform phononic materials made of non-resonant and resonant scatterers

Cite as: APL Mater. 9, 101101 (2021); doi: 10.1063/5.0059928
Submitted: 14 June 2021 • Accepted: 9 September 2021 •
Published Online: 4 October 2021

V. Romero-García,[1,a)] É. Chéron,[1] S. Kuznetsova,[1] J.-P. Groby,[1] S. Félix,[1] V. Pagneux,[1] and L. M. Garcia-Raffi[2]

AFFILIATIONS

[1] Laboratoire d'Acoustique de l'Université du Mans (LAUM), UMR 6613, Institut d'Acoustique - Graduate School (IA-GS), CNRS, Le Mans Université, Le Mans, France
[2] Instituto Universitario de Matemática Pura y Aplicada (IUMPA), Universitat Politècnica de València, València, Spain

Note: This paper is part of the Special Topic on Phononic Crystals at Various Frequencies.
[a)] **Author to whom correspondence should be addressed:** vicente.romero@univ-lemans.fr

ABSTRACT

Stealthy hyperuniform point patterns are characterized by a vanishing spatial Fourier transform around the origin of the reciprocal vector space. The long-range point density fluctuations are suppressed as well in materials consisting of such distribution of scatterers, opening up opportunities to control waves. Beside wave transport in such structured materials are driven by several elements, such as the acoustic properties of the host material, the scatterer characteristics, i.e., dimensions or resonant features, and the scatterer distribution patterns. The effects of these three basic elements on the wave transport properties are usually hard to discriminate. In this work, we analyze the transport properties of acoustic waves in one-dimensional phononic materials constituted of either non-resonant or resonant scatterers distributed along stealthy hyperuniform patterns in air. The pattern is controlled by the stealthiness, allowing us to continuously vary from random phononic materials to phononic crystals. The properties of the scatterers are controlled by their size and/or the resonant frequencies. The properties of the host material are controlled by the viscothermal losses. Transport properties of stealthy hyperuniform materials are found to be robust to both the scatterer dimensions and inherent viscothermal losses, while strongly affected by the scatterer resonances, which introduce sharp dips in the transmission coefficient.

I. INTRODUCTION

In recent years, the wave physics community has become increasingly interested in stealthy hyperuniform materials, as the dispersion relations of these materials exhibit isotropic bandgaps although they are not periodic.[1–13] These isotropic bandgaps have been exploited to design isotropic filters and free-shaped waveguides with both photonic[8,9] and phononic[6] hyperuniform materials. Stealthy hyperuniform materials are structured materials whose scatterer distribution induces the complete suppression of incident wave scattering for a set of wave vectors in the low frequency limit in the Born approximation.[14] In this sense, periodic structures like photonic[15] or phononic[16] crystals form a subset of stealthy hyperuniform materials. Waves propagating in a periodic medium are either diffracted by Bragg scattering or transmitted, thus introducing either Bragg peaks or zero regions in the structure factor.[17,18] Nevertheless, hyperuniformity further enhances the suppression of long-range point density fluctuations,[11] thus introducing correlated disorder to control waves. Waves propagating in these materials with correlated disorder present a phase diagram with transparent regions, Anderson localization, bandgaps, and wave diffusion.[5] Transport properties in one-dimensional (1D),[19] quasi-one-dimensional,[20] and higher dimensional systems have been controlled by correlated disorder, allowing the design of efficient non-resonant absorbers made of dilute disordered materials for broadband and omnidirectional waves.[21] Systems based on correlated disorder with target combination of transparent and non-transparent frequency regions for both electromagnetic[22] and

acoustic[23,24] waves have also been designed. The properties of stealthy materials appear to be robust to the losses present under realistic conditions, demonstrating the potential of correlated disorder for practical designs.

Wave transport in such materials is driven by several elements, such as the scatterer distribution patterns, the scatterer characteristics, i.e., dimensions or resonant features, and the acoustic properties of the host material. The effects of these three basic elements on the material transport properties are usually hard to discriminate. On the one hand, the concept of the stealthy hyperuniformity introduces an elegant way to design point patterns with finely tunable correlations encoded by the degree of stealthiness χ.[1–5,8,9,11–13] Asymptotic values of χ correspond to Poisson distribution, $\chi \to 0$, and perfect crystal lattices, $\chi \to 1$. More precisely, three structural regimes are distinguished[25,26] when χ increases: disordered, wavy-crystalline, and crystalline regimes.[26] Therefore, a continuous variation of χ from 0 to 1 induces a continuous change from the random point patterns to the periodic ones. On the other hand, the scatterers used for the design of stealthy hyperuniform materials in photonic[2,8,9] and phononic[6] systems are Mie resonators, the resonance of which is fixed close to the Bragg frequency by optimizing its dimensions for a given material. Recently, the effect of the local resonances in stealthy hyperuniform acoustic materials has been preliminary analyzed, showing a strong effect on the wave transport properties in the transparency band.[10] Moreover, in elastodynamics, the exact expressions for the effective properties of two-phase composites in the long-wavelength (quasistatic) regime via homogenized constitutive relations that are local in space have been applied to stealthy hyperuniform materials.[27] These local approximations have been extended beyond the quasistatic regime by postulating nonlocal formulas based on the similarities between electrodynamic and elastodynamic problems and the rigorous formulation of the nonlocal effective dynamic dielectric properties. By using these nonlocal microstructure-dependent approximations, it is shown that stealthy hyperuniform materials are less lossy than their nonhyperuniform counterparts in the quasistatic regime, and stealthy hyperuniform media can be perfectly transparent for a wide range of wavenumbers.[27,28] Finally, the presence of losses that cannot be avoidable in some types of waves, like the acoustic waves, is only accounted for in few works.[23]

In this work, we consider 1D phononic materials that allow us to easily discriminate such kinds of elements. Therefore, we discuss the fundamental effect of each element on the opening of bandgaps in stealthy hyperuniform materials. This allows us, for example, to place the resonance in different locations of the frequency spectrum even also outside of the transparency range and to analyze the possibly coupling with Bragg interferences, for instance. The point patterns are created by an optimization algorithm that minimizes the structure factor,[23,24] related to the scattering properties of the corresponding systems in the weak scattering approximation.[17,18] The wave transport properties are first analyzed in these 1D phononic structures going from disordered materials to ordered ones (phononic crystals) when χ varies continuously. We then compare these properties to those of the same 1D phononic materials when either non-resonant or resonant scatterers are located at the positions of the point patterns. We thus discuss the impact of the individual scattering properties of the scatterers constituting the whole material. We point out that the viscothermal losses, unavoidable in acoustics, are also accounted for. In practice, we use an air-filled square cross-sectional waveguide in which the stealthy hyperuniform materials made of non-resonant and resonant scatterers are embedded. A non-resonant scatterer consists of a local narrowing of the waveguide cross section such that it has a non-resonant behavior in the analyzed range of frequencies. A resonant scatterer consists of the same non-resonant scatterer but additionally loaded by a quarter-wavelength resonator.

II. STEALTHY HYPERUNIFORM POINT PATTERNS

A. Structure factor

Let us consider a distribution of N points placed at positions $\vec{r}_i$ $(i = 1, \ldots, N)$ inside a domain Λ in d-dimensions. The structure factor, $S(\vec{q})$, of this point pattern is defined as its spatial Fourier transform and reads as follows:

$$S(\vec{q}) = \frac{1}{N}\sum_{i=1}^{N}\sum_{j=1}^{N} e^{-i\vec{q}\cdot(\vec{r}_j-\vec{r}_i)}, \tag{1}$$

where $\vec{q}$ is a vector in the Fourier or reciprocal space.

The hyperuniformity concept can be defined by either the local number variance $\sigma^2(R)$ (i.e., the variance in the number of points within a randomly thrown spherical window of radius R) of the point pattern in the real space or the structure factor $S(\vec{q})$ in the reciprocal or Fourier space. In this work, we use the structure factor $S(\vec{q})$. Hyperuniform point patterns present a structure factor vanishing in the long-wavelength limit, i.e., $S(q \to 0) = 0$, where $q = |\vec{q}|$. One can define the stealthy hyperuniform point patterns as those presenting a structure factor that vanishes around the origin, $S(\Omega) = 0$ with Ω the set of $q \in [0, q_c]$.

To design the stealthy hyperuniform pattern, we use an optimization procedure, which looks for the positions $\vec{r}_i$ that minimizes the structure factor for a target region $q < q_c$ as described in Refs. 23 and 24. The algorithm provides a certain configuration starting from a random distribution. We can introduce a constraint as minimal distance l between scatterers by the following expression: $|\vec{r}_i - \vec{r}_j| \geq l \ \forall i \neq j$. This can be used as *a posteriori* to build realistic materials with finite size scatterers and thus to analyze the wave transport properties in realistic conditions. The objective functions to be simultaneously minimized are a summation of the structure factor

$$\phi(\vec{r}_1, \ldots, \vec{r}_N) = \sum_{q<q_c} S(q) \tag{2}$$

and the standard deviation function

$$\Sigma = \sqrt{\frac{1}{N-1}\sum_{q<q_c}\left|S(q) - \frac{1}{N}\sum_{q<q_c} S(q)\right|^2}. \tag{3}$$

We note that the distribution of points obtained by this optimization procedure is equivalent to those obtained by the collective-coordinate optimization technique described in Refs. 12, 14, 25, and 26 when $l = 0$.

B. Stealthiness

In this section, we define the stealthiness, χ, which characterizes the point pattern that meets the hyperuniformity definition. The

stealthiness is the ratio of the number $M(\Omega)$ of the constrained vectors in Ω to the number of degrees of freedom in the real space $d(N-1)$ in d-dimensions (if the system translational degrees of freedom are removed). We consider a 1D domain of length L and Ω becomes a segment of length q_c. Therefore, $M(\Omega) = (q_c L/2\pi)$, and for $N \gg 1$,

$$\chi \simeq \frac{q_c L}{2\pi N}. \tag{4}$$

We note that χ is bounded in the domain $[0,1]$ if q_c is in the interval $[0, 2\pi N/L]$. Note also that the expression of χ for higher dimensions is strongly dependent on the shape of the domain Ω.[7,13]

Let us define here the set $C(\chi)$ that will stand for the set of configurations $\vec{r}_i$ with $i = 1, \ldots, N$ that satisfies $S(q < 2\pi N\chi/L) = 0$. It is clear that $C(\chi = 0)$ includes all the point pattern configurations and that $C(\chi_1) \subseteq C(\chi_2)$ with $\chi_1 \geq \chi_2$. The local dimension of $C(\chi)$ is given by $\max(N(1-2\chi), 1)$ for $0 \leq \chi < 1$.[25]

C. χ-dependence of the structure factor

In this section, we analyze the structure factor of different stealthy hyperuniform point patterns generated with different values of χ. The minimum distance between points is fixed at $l = L/100$, i.e., $|\vec{r}_i - \vec{r}_j| \geq L/100 \ \forall i \neq j$. Thus, the generated point patterns will allow the use of finite width scatterers in a second step. We consider $N = 25$ points as an example. Figure 1(a) shows the map of the $\log(S(\vec{q}))$ in terms of χ and $qL/2\pi N$. The red continuous line delimits the constrained frequency region imposed by the value of χ. As demonstrated in Ref. 25, three regions are identified when $N \gg 1$: (i)$0 \leq \chi \lesssim 1/3$, (ii)$1/3 \lesssim \chi < 1/2$, and (iii)$1/2 \leq \chi < 1$. We note here that the behavior for higher dimensions is similar with three regions named as "disordered", "wavy-crystalline," and "crystalline."[26] For clarity, we start by analyzing the lower and upper regions corresponding to the two bounds of χ.

In region (i), $0 \leq \chi \lesssim 1/3$, the structure factor behavior is twofold: For $q \leq q_c$, the values of the structure factor are orders of magnitude smaller than those for $q > q_c$. As an example of typical behavior, both the point pattern and the structure factor calculated for $\chi = 0.2$, as indicated by the horizontal dashed black line in Fig. 1(a), are depicted in Fig. 1(b). The point patterns in this region are disordered and the optimization problem is highly degenerated due to the high dimension of the set $C(\chi)$.

In region (iii), $1/2 \leq \chi < 1$, the unique solution of the minimization problem is the periodic pattern.[25] The local dimension of $C(\chi)$ is 1, corresponding to the periodic point distribution. The structure factor map depicted in Fig. 1(a) presents the Bragg peaks[17,18] at $q_B = n2\pi N/L$, with $n \in \mathbb{Z}$. The point pattern crystalizes in a 1D array whose periodicity is $a = L/N$. In this case, $\vec{q}_B$ represents the well-known vectors of the reciprocal lattice in the reciprocal space of the periodic system.

In region (ii), $1/3 \lesssim \chi < 1/2$, the point pattern undergoes a transition from disordered to a periodic pattern and combines the properties of the other two regions. The structure factor smoothly mixes the behavior of region (*i*), in which it is minimized only for $q < q_c$, and that of region (iii), in which it is minimized for all q different than those corresponding to Bragg peaks. Therefore, the structure factor alternates between minimal and non-minimal

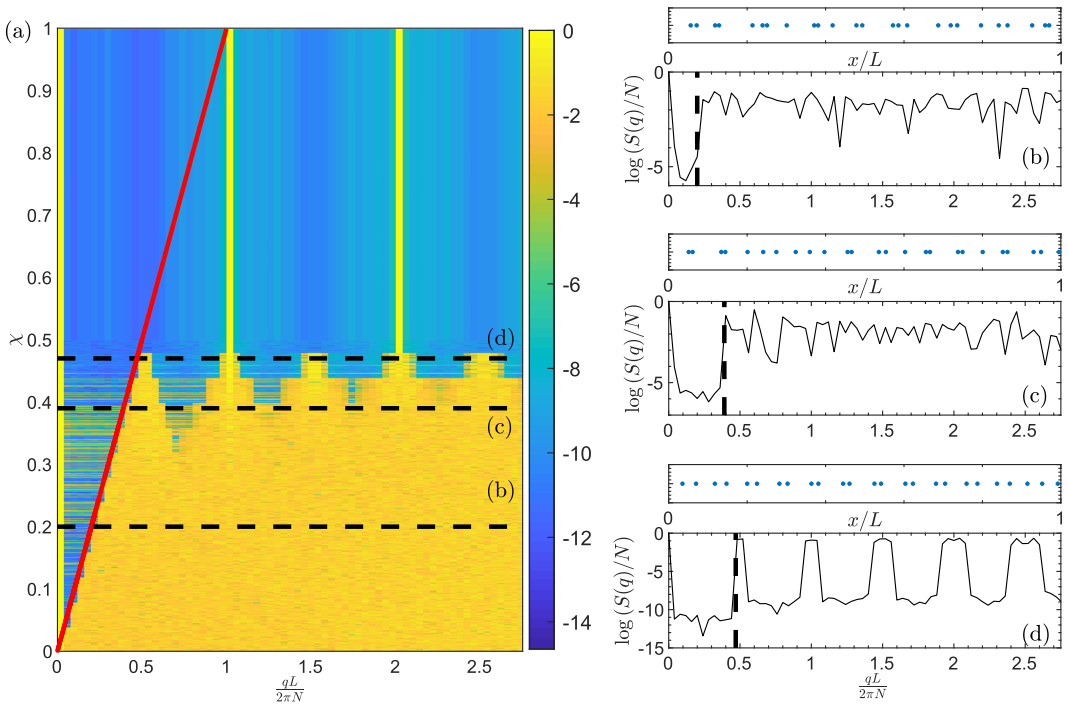

FIG. 1. (a) $\log(S(\vec{q}))$ in terms of χ and $qL/2\pi N$ for a 1D configuration with $N = 25$ points in $L = 1$ m considering the constraint $l = L/100$ m. A continuous red line represents the limit imposed by χ. (b)–(d) Examples for $\chi = 0.2$, 0.39, and 0.47, respectively, corresponding to the horizontal dashed lines shown in (a). Vertical thick dashed black lines in (b)–(d) show the frequency limits imposed by χ. Upper panels in (b)–(d) show the corresponding stealthy hyperuniform point patterns.

values. To illustrate this dynamic, the point distribution and the structure factor for $\chi = 0.39$ and $\chi = 0.47$, as indicated by the two horizontal dashed black lines in Fig. 1(a), are represented in Figs. 1(c) and 1(d). For the case $\chi = 0.39$, $S(\vec{q})$ is minimum in the region $q < q_c$, but other minima appear. For $\chi = 0.47$, which is a value very close to the limit of this region, $S(\vec{q})$ presents in addition smooth alternation of minima and maxima for $q > q_c$.

The structure factor for stealthy hyperuniform point patterns in the absence of constraint on l is analyzed in the supplementary material. Its overall behavior is preserved. The three χ-dependent regions appear at the same limits. However, it should be noticed here that the minima of $S(q)$ are much clearer than in the constrained case presented in this section.

III. WAVE TRANSPORT PROPERTIES IN STEALTHY HYPERUNIFORM PHONONIC MATERIALS

Wave transport is calculated by using the transfer matrix method as explained in the supplementary material. With the 1D stealthy hyperuniform acoustic material being an asymmetric and reciprocal structure, it is successively excited by a plane wave from one side and then from the other side in order to evaluate the scattering coefficients, i.e., the two reflection coefficients, R^+ and R^-, and the transmission coefficient T. The eigenvalues of the transfer matrix provide the dispersion relation of the material, the supercell of which is composed of N scatterers arranged on the stealthy hyperuniform pattern. Problems are solved with and without viscothermal losses. Losses are accounted for via effective complex and frequency dependent density and bulk modulus as given in Ref. 29.

A. 1D stealthy hyperuniform acoustic materials

We consider a 1D stealthy acoustic material consisting of an air-filled waveguide of square cross section presenting $N = 25$ scatterers. These scatterers are either non-resonant, made of identical rectangular cross section scatterers (reduction of the main waveguide section along a single direction), or resonant, made of these rectangular cross section scatterers additionally loaded by identical quarter-wavelength resonators (see Fig. 2 for details). The waveguide side W is chosen such that only plane waves propagate, i.e., the frequencies are lower than the first cutoff frequency of the waveguide. The rectangular cross section scatterer consists in a reduction of the waveguide cross section along a single direction of thickness $l_d \equiv l$; therefore, the rectangular cross section scatterer presents a width W and height $h_d = \zeta_d \times W$, where $\zeta_d \leq 1$ is the height (section) reduction ratio. The quarter-wavelength resonator consists in a cylindrical tube of radius $R_q = l_d/4$ and length l_q. Its resonance frequency is $f_s \simeq c_q/4l_q$, where c_q is the sound speed of the fluid in the cylindrical tube. The scatterers are arranged on the stealthy hyperuniform pattern, $\vec{r}_i \equiv x_i$ in the 1D domain Λ, analyzed previously (constraint $l = L/100$). The length of the 1D domain is $L = 1$ m and the side is $W = 1.5$ cm. The scatterer thickness is fixed at $l_d = L/100 = 1$ cm, thus fixing the radius of the quarter-wavelength $R_q = 2.5$ mm. The scattering intensity of the non-resonant scatterers is varied by modifying the section reduction ratio $\zeta_d = [0.33, 0.5, 0.66, \text{and } 0.83]$. The

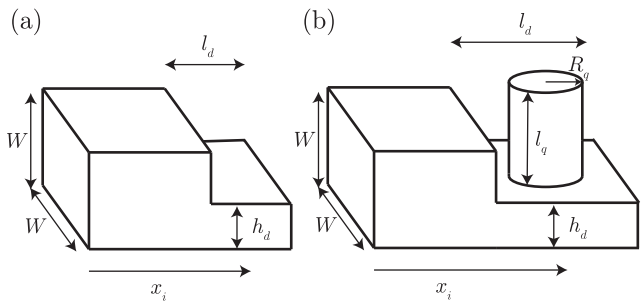

FIG. 2. Sketches of (a) the non-resonant scatterer made of a rectangular cross section tube width W and height $h_d = \zeta_d W$ and length l_d and (b) the resonant scatterer where quarter-wavelength resonators of radius R_q and length l_q load the non-resonant scatterer. These scatterers will be located at the position x_i given by the stealthy hyperuniform point patterns forming the stealthy hyperuniform materials.

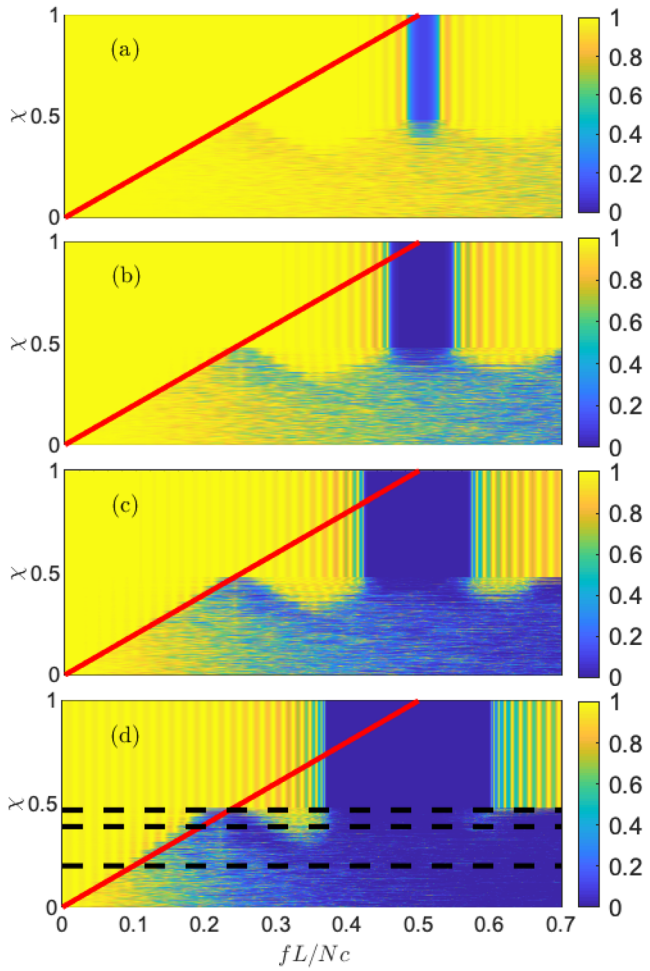

FIG. 3. (a)–(d) Maps of transmission coefficient, $|T|$, in terms of χ and normalized frequency fL/Nc for $\zeta_d = 0.83$ (a), $\zeta_d = 0.66$ (b), $\zeta_d = 0.5$ (c), and $\zeta_d = 0.33$ (d). The red continuous lines correspond to the limit imposed by χ, Eq. (4), $f_c = \chi Nc/2L$. Horizontal dashed lines in (d) represent the analyzed cases in Fig. 4. The analysis of this figure is done without considering the losses.

quarter-wavelength resonators load the rectangular cross section scatterer with $\zeta_d = 0.33$. The length of the quarter-wavelength resonator l_q is modified such that the resonance frequency takes the values $f_s = [1, 1/2, 1/3]f_B$, where $f_B = cN/2L$ is the Bragg frequency corresponding to the L/N-periodic array (c is the sound speed of the host material, i.e., of the square cross-sectional waveguide).

B. Non-resonant scatterers

We start by analyzing the transmission coefficients $|T|$ of the different proposed stealthy hyperuniform materials consisting of non-resonant scatterers without considering the viscothermal losses. The maps of $|T|$ in terms of χ and normalized frequency fL/Nc are depicted in Figs. 3(a)–3(d) for $\zeta_d = [0.83, 0.66, 0.5, \text{and } 0.33]$, respectively. The red continuous lines show the cutoff frequency imposed by χ, i.e., $f_c = \chi Nc/2L$. When the scatterers are small, i.e., $\zeta_d = 0.83$ [Fig. 3(a)], the scattering is weak and the transmission coefficient is mainly affected by the Bragg interferences when $\chi > 0.45$. The three χ-dependent regions described in Sec. II C are weakly visible.

The scattering intensity increases together with the impedance mismatch between the rectangular cross section scatterer and the main tube, i.e., with the decrease of ζ_d. The transmission coefficient is thus more impacted by the pattern, as can be seen in Figs. 3(b)–3(d). The bandgap width of the periodic distributions ($\chi \geq 0.5$) decreases with the ratio ζ_d. The transparency regions for $f < f_c$ are clearly visible in Figs. 3(b)–3(d). This transparency zone is one of the main characteristics of the stealthy hyperuniform materials and is a direct translation of the constraints imposed on the structure factor. We can clearly see how the spatial distribution of the scatterers impacts the transmission coefficient in each of the three regions: for $\chi \lesssim 1/3$, where the point pattern is mostly disordered without any hint of periodicity, we see the transparency for $f \leq f_c$ and the low transmission coefficient region for $f > f_c$; for $\chi \geq 1/2$, we can see that only the region around the Bragg frequency is impacted by the scattering; for $1/3 \lesssim \chi < 1/2$, the characteristic transition zone with the alternating transparent and nontransparent zones as imposed by the structure factor is shown.

Both the scattering properties and the dispersion relation (eigenvalues of the transfer matrix when periodic conditions are imposed at the limits of the material) are now investigated in more detail in Fig. 4 when $\zeta_d = 0.33$ corresponding to the case in which the different regions are clearly present. Figures 4(a)–4(c) show the reflection and the transmission coefficients when

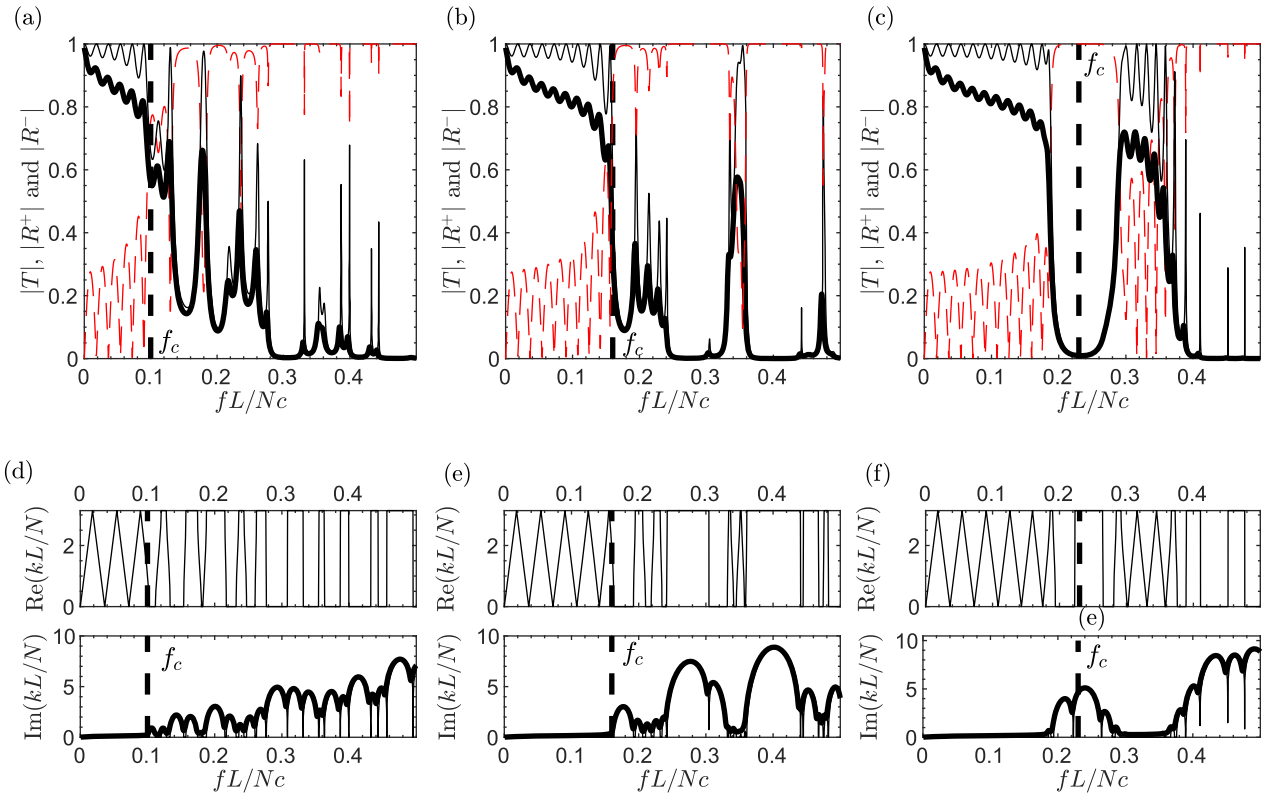

FIG. 4. Wave transport properties of stealthy hyperuniform materials made of non-resonant scatterers in the position of the stealthy hyperuniform point distributions with $\chi = [0.2, 0.39, \text{and } 0.47]$ as indicated in Fig. 3(d) when $\zeta_d = 0.33$. We note here that the range of frequencies is reduced with respect to the one of Fig. 3(d) in order to highlight the main physical phenomena. (a)–(c) Red dashed and black continuous lines show the reflection, $|R^+| = |R^-|$, and transmission, $|T|$, coefficients. The thick black continuous line represents the transmission coefficient calculated in the presence of viscothermal losses. (d)–(f) Real (upper panel) and imaginary (lower panel) parts of the dispersion relation for $\chi = [0.2, 0.39, \text{and } 0.47]$, respectively. Vertical thick dashed black lines represent the limits imposed by χ, $f_c = \chi Nc/2L$. The thick line in the lower panel shows the imaginary part of the dispersion relation calculated with losses.

$\chi = [0.2, 0.39, \text{and } 0.47]$, respectively [as highlighted by the horizontal lines in Fig. 3(d)].

First, these properties are analyzed in the absence of losses. In that case, $R^+ \neq R^-$ because the structure is asymmetric, but $|R^+| = |R^-|$ because of energy conservation. The cutoff frequency f_c imposed by χ is shown by the vertical thick dashed black lines in Figs. 4(a)–4(c). The scattering coefficient behavior is clearly different if f is lower or larger than f_c. When $f \leq f_c$, the characteristic Fabry–Pérot peaks are visible in the scattering parameters. They are due to the finite size L of the sample, the effective impedance of which is different from that of the surrounding medium. When $f > f_c$, no Fabry–Pérot peaks are noticed. In particular, the alternation of transparent and non-transparent regions translates the transition between the disordered and periodic distribution of scatterers when $\chi \simeq 0.5$ [see Fig. 4(c)].

Figures 4(d)–4(f) show the complex dispersion relation calculated for $\chi = [0.2, 0.39, \text{and } 0.47]$ considering the system with $N = 25$ as a supercell with periodicity L (see the supplementary material for more details). A different behavior is again observed depending on whether f is lower or higher than f_c. When $f \leq f_c$, the system presents, for all the analyzed cases, a dispersion relation with near zero imaginary part of k and a linear dispersion relation for the real part. When $f > f_c$ and $\chi \lesssim 1/3$ [Fig. 4(d)], the real part of the dispersion relation is characterized by flat bands. These modes are mostly localized in the structure due to the disordered feature of the system. When $1/3 \lesssim \chi < 1/2$ [see Fig. 4(e)], regions with flat bands alternate with dispersive bands in the real part, which correspond to the alternation of the transparent and opaque frequency regions in the transmission coefficient. We note that the system becomes dispersive close to f_c when $\chi > 0.5$ (due to the periodicity imposed by the crystallization). That is the reason why the calculated limit f_c [vertical thick dashed black line in Fig. 4(f)] considering c the speed of sound in air fits with neither the frequency at which the dispersion relation starts to present an imaginary part [see Fig. 4(f)] nor the beginning of the opaque region in scattering coefficients in Fig. 4(c).

The effect of viscothermal losses in the system is now analyzed. Thick black continuous lines in Fig. 4 show both the transmission coefficient $|T|$ and the imaginary part of the dispersion relation calculated considering the complex and frequency dependent density and bulk modulus in each part of the waveguide. The transparency region when $f \leq f_c$ is impacted by the viscothermal losses but as shown by the dispersion relation is robust to losses. We note that the decrease of $|T|$ is very close to that in an empty waveguide as shown in Ref. 23. When $f > f_c$, the peaks of the transmission coefficient, due to the low dispersion bands of the dispersion relation, are strongly affected and the amplitude is reduced. In this case, we note that due to the viscothermal losses $|R^+| \neq |R^-|$ although the results are not shown in the figure for simplicity.

C. Resonant scatterers

In this section, we introduce both the resonance effect and the viscothermal losses into the system. We analyze its

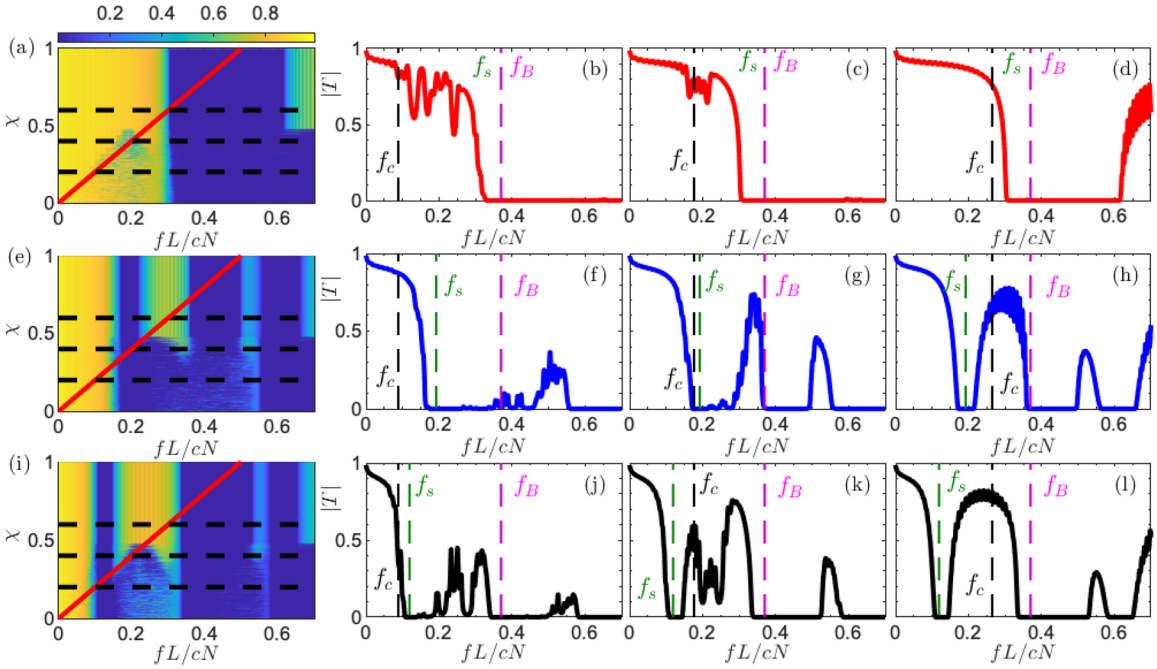

FIG. 5. Analysis of the acoustic transmission coefficient of resonant stealthy hyperuniform materials for (a)–(d) $f_s = f_B$, (e)–(h) $f_s \simeq f_B/2$, and (i)–(l) $f_s \simeq f_B/3$ for the configuration with $\zeta_d = 0.33$. Maps of transmission coefficient, $|T|$, in terms of χ and normalized frequencies fL/Nc for $f_s = [1, 1/2, 1/3]\, f_B$ is shown in (a), (e), and (i), respectively. (b)–(d), (f)–(h), and (j)–(l) show the transmission coefficient for the case $\chi = [0.2, 0.4, 0.5]$, respectively, for $f_s = f_B$, $f_s = f_B/2$, and $f_s = f_B/3$. The viscothermal effects of the system have been considered for all the calculations.

transmission coefficients depending on both χ and f_s for the case $\zeta_d = 0.33$. Figures 5(a), 5(e), and 5(i) show the map of $|T|$ in terms of χ and the normalized frequency fL/cN for three different resonance frequencies, $f_s = [1, 1/2, 1/3]f_B$, respectively. For each case, we evaluate the transmission coefficient for $\chi = [0.2, 0.4, 0.55]$ placed in the three regions of interest shown and described in Sec. III A. Figures 5(b)–5(d), 5(f)–5(h), and 5(j)–5(l) show $|T|$ for $\chi = [0.2, 0.4, 0.55]$ and for $f_s = f_B$, $f_s = f_B/2$, and $f_s = f_B/3$.

We start by analyzing the case $f_s = f_B$ [Figs. 5(a)–(d)]. For $\chi > 0.5$, the system crystalizes and produces a phononic crystal with periodicity L/N. The coupling of the resonance frequency and the Bragg interferences produces the well-known widening of the bandgap,[30,31] which is clearly shown in both Figs. 5(a) and 5(d). In order to compare, we refer to the non-resonant case shown in Fig. 3(d). If we now reduce the value of the stealthiness, the region of low transmission coefficient strongly increases in frequency as shown in Figs. 5(b) and 5(c): the high frequency transmission range shown in the periodic case is suppressed as periodicity is removed. For example, for $\chi = 0.2$, the bandgap starts at $fL/cN = 0.35$, showing a broad range of frequencies with very low values of transmission coefficient for higher frequencies of the analyzed range. For all the cases, we notice that the transparency region imposed by χ is preserved.

Figures 5(e)–5(h) show the analysis for the case $f_s = f_B/2$. For the purely periodic case, shown in Fig. 5(e) and in Fig. 5(h), three dips of the transmission coefficient can be identified for $\chi \geq 0.5$: two corresponding to the fundamental and first harmonic of the resonator and one corresponding to the Bragg interferences. For the case $\chi = 0.4$, shown in Fig. 5(g), we need to revisit the results of the non-resonant stealthy material [see Fig. 4(c)]. For this region, a dip of the transmission coefficient is shown for $f = f_B/2$. Now, the resonator is tuned at this particular frequency, thus showing a similar effect of the bandgap widening but at $f = f_B/2$. The coupling between the resonance and the quasi-double periodicity of the system creates a wide bandgap at this particular region. Finally, for the case $\chi = 0.2$ shown in Fig. 5(f), the disorder on the system together with the resonance frequencies of the resonator (first and second harmonics) produces considerable reduction of the amplitude of the transmission coefficient from $fL/Nc = 0.18$.

Finally, Figs. 5(i)–5(l) show the analysis for the case $f_s = f_B/3$. Again, for the periodic case [Fig. 5(l)], we see the three dips for the transmission coefficient as in the previous case. For the case with $\chi = 0.4$, $|T|$ shows four regions with very low values: the first and second bands due to the double periodicity and the first and second harmonics of the resonators. For the case with $\chi = 0.2$, the correlated disorder in the system reduces the transparency ranges between dips of the transmission coefficient.

IV. CONCLUSION

The wave transport properties of 1D phononic materials made of stealthy hyperuniform distributions of non-resonant or resonant scatterers are analyzed in this work. The stealthiness is used to continuously analyze the properties from random distribution to periodic ones. In the reciprocal space, there are three regimes characterizing the point patterns. The disordered region, (i) $0 \leq \chi \lesssim 1/3$, is characterized by transparent and opaque frequency regions with the cutoff frequency imposed by χ. The wavy-crystalline region, (ii) $1/3 \lesssim \chi < 1/2$, is characterized by both the transparent frequency range imposed by χ and an alternation of opaque and transparent frequency regions depending on the value of χ. We note that in this region, the point pattern shows a dimerization made of two sublattices with periodicity $2L/N$ when χ approaches to 0.5. The last region is the crystalline, (iii) $1/2 \leq \chi < 1$, in which the Bragg peaks are clearly visible and the point distribution is purely periodic. Once the point pattern is built and analyzed, the phononic material is made by adding non-resonant and resonant scatterers at these positions. The material is made by an air-filled waveguide in which the cross section is adapted to be always in the plane wave regime. The investigations for the non-resonant scatterers show that the behavior of the structure factor is well-captured by the scattering coefficients of the system. However to clearly identify the three regions, a given impedance mismatch is necessary. Interestingly, the lossless system exhibits purely real dispersion relation in the transparent region imposed by χ. The wave transport properties are shown to be robust to the presence of viscothermal losses. The response of the system made of resonant scatterers is richer due to the fact that the resonance of the individual scatterers, f_s, is added to the system and can be exploited to couple with the scattering effects provided by the point pattern. When $f_s \simeq f_B$, while the effect of superbandgap is observed for periodic structures $\chi \geq 1/2$, for $\chi < 1/2$, a broader deep of the transmission coefficient appears from f_s. Moreover, when $f_s \simeq f_c$, wide deeps of the transmission coefficient are also created. If the resonance is placed away of f_c or f_B, the resonance and the scattering due to the point pattern can be combined independently to produce frequency ranges with low amplitude of the transmission coefficient. In particular, the disordered systems with resonant scatterers present better performances to be used as acoustic isolation systems than the periodic ones when losses are considered.

SUPPLEMENTARY MATERIAL

See the supplementary material for the detailed description of the transfer matrix method used to analyze the stealthy hyperuniform materials described in this work. The analysis of the structure factor for stealthy hyperuniform materials generated without constraints, i.e., with $l = 0$, is also shown.

ACKNOWLEDGMENTS

This work was funded by the project HYPERMETA under the program Étoiles Montantes of the Région Pays de la Loire, by the ANR-RGC METARoom (Grant No. ANR-18-CE08-0021) project, and by Project No. PID2020-112759GB-I00/AEI/10.13039/501100011033 of the Ministerio de Ciencia e Innovación.

The authors have no conflicts to disclose.

DATA AVAILABILITY

The data that support the findings of this study are available from the corresponding author upon reasonable request.

REFERENCES

[1]T. Amoah, "Designer disordered complex media: Hyperuniform Photonic and phononic band gap materials," Ph.D. thesis, Advanced Technology Institute and Department of Physics, Faculty of Engineering and Physical Science, University of Surrey, 2016.

[2]G. J. Aubry, L. S. Froufe-Pérez, U. Kuhl, O. Legrand, F. Scheffold, and F. Mortessagne, "Experimental tuning of transport regimes in hyperuniform disordered photonic materials," Phys. Rev. Lett. **125**, 127402 (2020).

[3]M. Florescu, S. Torquato, and P. J. Steinhardt, "Designer disordered materials with large, complete photonic band gaps," Proc. Natl. Acad. Sci. U. S. A. **106**, 20658–20663 (2009).

[4]L. S. Froufe-Pérez, M. Engel, P. F. Damasceno, N. Muller, J. Haberko, S. C. Glotzer, and F. Scheffold, "Role of short-range order and hyperuniformity in the formation of band gaps in disordered photonic materials," Phys. Rev. Lett. **117**, 053902 (2016).

[5]L. S. Froufe-Pérez, M. Engel, J. J. Sáenz, and F. Scheffold, "Band gap formation and Anderson localization in disordered photonic materials with structural correlations," Proc. Natl. Acad. Sci. U. S. A. **114**, 9570 (2017).

[6]G. Gkantzounis, T. Amoah, and M. Florescu, "Hyperuniform disordered phononic structures," Phys. Rev. B **95**, 094120 (2017).

[7]O. Leseur, R. Pierrat, and R. Carminati, "High-density hyperuniform materials can be transparent," Optica **3**, 763–767 (2016).

[8]W. Man, M. Florescu, E. P. Williamson, Y. He, S. R. Hashemizad, B. Y. C. Leung, D. R. Liner, S. Torquato, P. M. Chaikin, and P. J. Steinhardt, "Isotropic band gaps and freeform waveguides observed in hyperuniform disordered photonic solids," Proc. Natl. Acad. Sci. U. S. A. **110**, 15886–15891 (2013).

[9]W. Man, M. Florescu, K. Matsuyama, P. Yadak, G. Nahal, S. Hashemizad, E. Williamson, P. Steinhardt, S. Torquato, and P. Chaikin, "Photonic band gap in isotropic hyperuniform disordered solids with low dielectric contrast," Opt. Express **21**, 19972–19981 (2013).

[10]A. Rohfritsch, J.-M. Conoir, T. Valier-Brasier, and R. Marchiano, "Impact of particle size and multiple scattering on the propagation of waves in stealthy-hyperuniform media," Phys. Rev. E **102**, 053001 (2020).

[11]S. Torquato and F. H. Stillinger, "Local density fluctuations, hyperuniformity, and order metrics," Phys. Rev. E **68**, 041113 (2003).

[12]S. Torquato, G. Zhang, and F. H. Stillinger, "Ensemble theory for stealthy hyperuniform disordered ground states," Phys. Rev. X **5**, 021020 (2015).

[13]S. Torquato, "Hyperuniformity and its generalizations," Phys. Rev. E **94**, 022122 (2016).

[14]R. D. Batten, F. H. Stillinger, and S. Torquato, "Classical disordered ground states: Super-ideal gases and stealth and equi-luminous materials," J. Appl. Phys. **104**, 033504 (2008).

[15]J. D. Joannopoulos, S. G. Johnson, J. N. Winn, and R. D. Meade, *Photonic Crystals: Molding the Flow of Light* (Princeton University Press, 2008).

[16]*Acoustic Metamaterials and Phononic Crystals*, edited by P. Deymier (Springer, 2013).

[17]N. W. Ashcroft and N. D. Mermin, *Solid State Physics* (Holt, Rinehart and Winston, 1976).

[18]C. Kittel, *Introduction to Solid State Physics*, 8th ed. (Wiley, 2004).

[19]F. M. Izrailev, A. A. Krokhin, and N. M. Makarov, "Anomalous localization in low-dimensional systems with correlated disorder," Phys. Rep. **512**, 125–254 (2012).

[20]I. F. Herrera-González, J. A. Méndez-Bermúdez, and F. M. Izrailev, "Transport through quasi-one-dimensional wires with correlated disorder," Phys. Rev. E **90**, 042115 (2014).

[21]A. Sheremet, R. Pierrat, and R. Carminati, "Absorption of scalar waves in correlated disordered media and its maximization using stealth hyperuniformity," Phys. Rev. A **101**, 053829 (2020).

[22]U. Kuhl, F. M. Izrailev, A. A. Krokhin, and H.-J. Stöckmann, "Experimental observation of the mobility edge in a waveguide with correlated disorder," Appl. Phys. Lett. **77**, 633–635 (2000).

[23]V. Romero-García, N. Lamothe, G. Theocharis, O. Richoux, and L. García-Raffi, "Stealth acoustic materials," Phys. Rev. Appl. **11**, 054076 (2019).

[24]S. Kuznetsova, J. P. Groby, L. M. Garcia-Raffi, and V. Romero-García, "Stealth and equiluminous materials for scattering cancellation and wave diffusion," Waves Random Complex Media (published online, 2021).

[25]Y. Fan, J. K. Percus, D. K. Stillinger, and F. H. Stillinger, "Constraints on collective density variables: One dimension," Phys. Rev. A **44**, 2394–2402 (1991).

[26]O. U. Uche, F. H. Stillinger, and S. Torquato, "Constraints on collective density variables: Two dimensions," Phys. Rev. E **70**, 046122 (2004).

[27]J. Kim and S. Torquato, "Effective elastic wave characteristics of composite media," New J. Phys. **22**, 123050 (2020).

[28]S. Torquato and J. Kim, "Nonlocal effective electromagnetic wave characteristics of composite media: Beyond the quasistatic regime," Phys. Rev. X **11**, 021002 (2021).

[29]M. R. Stinson, "The propagation of plane sound waves in narrow and wide circular tubes, and generalization to uniform tubes of arbitrary cross-sectional shape," J. Acoust. Soc. Am. **89**, 550–558 (1991).

[30]C. E. Bradley, "Time harmonic acoustic Bloch wave propagation in periodic waveguides. Part I. Theory," J. Acoust. Soc. Am. **96**, 1844–1853 (1994).

[31]N. Sugimoto and T. Horioka, "Dispersion characteristics of sound waves in a tunnel with an array of Helmholtz resonators," J. Acoust. Soc. Am. **97**, 1446–1459 (1995).